Corrosion monitoring and performance evaluation of protective coatings driven by electrochemical technology

Artur Zieliński[1]

[1]Gdańsk University of Technology, Gdansk, Poland

***Corresponding Author:**
artur.zielinski@pg.edu.pl

Received: 04/08/2024
Revised: 29/12/2024
Accepted: 01/05/2025
Published: 26/10/2025

Abstract: Protective coatings offer low cost, ease of application, high efficiency, and broad applicability, making them an effective method for safeguarding metal structures. This study simulates the electrochemical corrosion behavior of a composite coating (graphene/fluorocarbon coating) in seawater and evaluates its hardness, adhesion, and impact resistance. During simulation, polarization curves and AC impedance spectroscopy were employed to monitor the coating's electrochemical corrosion and failure processes. Experimental results indicate that graphene provides an excellent barrier against corrosive media. The protective performance of the coating first increases and then decreases with increasing graphene content. At a content of 0.5% (mass fraction), the coating exhibits a corrosion current density of 2.366×10^{-10} A/cm^2, demonstrating the best corrosion resistance. Furthermore, the entire 360-hour immersion period was classified as the early immersion stage, indicating effective isolation against corrosive liquid penetration and optimal protective performance for the Q235 steel substrate. The FEVE-0.5%G coating exhibits moderate hardness, good adhesion, and erosion resistance, providing a certain level of protective efficacy.

Keywords: protective coating, polarization curve, AC impedance spectroscopy, electrochemical corrosion

1 | Introduction

Corrosion remains a persistent and severe issue in industrial settings, significantly impairing the performance and lifespan of various facilities and equipment [1]. Industrial corrosion not only adversely affects production efficiency and maintainability but also poses potential threats to environmental safety and personnel [2]. The corrosion resistance of protective coatings has been a subject of considerable attention, as coating-based corrosion protection is widely applied across multiple industrial sectors, including chemical, petroleum, natural gas, water treatment, and power generation [3, 4].

Addressing limitations such as the finite longevity of corrosion inhibitors, vulnerability of metallic coatings to damage, and the power source dependency of electrochemical protection, organic coatings offer long-term corrosion protection independent of time and environment. Their uniform coverage on metal surfaces reduces the risk of exposing damaged areas to corrosion [5, 6]. This is particularly relevant in transportation and

infrastructure sectors, including automobiles, aircraft, vessels, pipelines, bridges, and buildings [7]. Polymer-based anticorrosive coatings are typically classified by resin or binder type, including epoxy, polyurethane, acrylic, and alkyd resins [8]. Most organic coatings are applied as liquids and cured through coating processes, making organic solvents a primary component in polymer-based anticorrosive formulations. However, research on coating modification alone can no longer meet the demands of modern application environments. Numerous scholars have shifted their focus to corrosion monitoring, providing robust data and technical support for targeted anti-corrosion strategies [9, 10].

Corrosion monitoring technologies can identify areas of early corrosion occurrence, facilitating timely detection and maintenance. Currently, two common corrosion monitoring techniques are employed: one relies on color changes of indicators, including acid-base indicators and metal ion indicators [11, 12]. Acid-base indicators are typically organic weak acids or weak bases, such as phenolphthalein and methyl orange, which exist in different forms under varying pH conditions, thereby displaying different colors [13]. Metal ion indicators are generally substances that form complexes or precipitates with metal ions, such as thiocyanate ions for detecting iron ions, which form a red complex with iron ions [14]. Another approach involves monitoring via fluorescent agents, such as organic compounds like anthraquinones, azo compounds, and quinolines. Based on their response mechanisms, fluorescent agents can be categorized into fluorescence-generating and fluorescence-quenching types. Based on the mechanism of action, fluorescent agents can be categorized into two scenarios: one type exhibits a pronounced response to local pH changes at the corrosion site, binding with H^+ or OH^- to form new fluorescent compounds, thereby monitoring pH variations and the extent of corrosion. Examples include calcein and 5,6-carboxyfluorescein [15, 16]. The other type exhibits a pronounced response to changes in metal ion concentration within the corrosion zone, such as quinoline. These fluorescent substances form chelate complexes with metal ions, thereby generating a fluorescent effect [17, 18].

Liu et al. [19] reported a protective coating capable of self-monitoring corrosion, primarily composed of pH-sensitive multilayer chitosan/alginate-coated $CaCO_3$ microcapsules. These capsules release corrosion indicators upon sensing changes in environmental pH, enabling corrosion damage detection. Tian et al. [20] investigated the monitoring efficacy of rhodamine-ethylenediamine for corrosion of copper artifacts protected by epoxy coatings using fluorescence microscopy and electrochemical impedance spectroscopy. Their experiments demonstrated that incorporating just 0.8 wt% rhodamine-ethylenediamine into the epoxy coating enables effective monitoring of metal corrosion in copper artifacts.

Furthermore, with advancements in digital technology, monitoring methods based on unmanned technology and sensor technology have begun to emerge. Sun et al. [21] reviewed the application of unmanned platform technology in corrosion monitoring, identifying its potential to enhance the efficiency, accuracy, and safety of corrosion monitoring beneath coatings, thereby guiding the development direction of metal corrosion resistance research. Wang et al. [22] employed atmospheric corrosion monitoring (ACM) technology to compare the corrosion resistance trends over time between epoxy coatings and epoxy coatings containing zinc phosphate corrosion inhibitors. Results demonstrated that the ACM-measured electrocorrosion currents were consistent with conventional electrochemical measurements. Latif et al. [23] developed a coating corrosion detection system using micro-sensors, applicable to remote, fixed, and mobile devices. It monitors corrosion beneath coatings and stress variations on coatings via linear programming methods and coating microstrain calculation techniques. Davis et al. [24] proposed a corrosion protection and condition monitoring technology based on smart patches. This approach utilizes fluoropolymer films incorporating sensor electrodes and pressure-sensitive adhesive, enabling corrosion state detection through electrochemical impedance spectroscopy measurements. Zamarreño et al. [25] focused on reinforced concrete structures, summarizing the mechanisms by which

various optical sensor technologies and devices monitor corrosion. Specifically, they measured the quantity of corrosion byproducts to provide effective information such as corrosion severity. Cook [26] noted that Mössbauer spectroscopy can identify different iron oxides forming rust on corroded steel in marine and other environments and map them within rust coatings, aiding in advancing corrosion research.

While monitoring using color-changing indicators is relatively straightforward, factors such as a wide color change range and difficulty in distinguishing color variations can interfere with corrosion monitoring. In contrast, fluorescent agents offer high monitoring sensitivity and measurement accuracy, enabling more precise evaluation and monitoring of corrosion trends and severity [27, 28]. In-situ corrosion monitoring sensors for metal components are primarily used for long-term monitoring of corrosion rates, demanding high sensor longevity and long-term stability. Electrochemical sensors for in-situ corrosion monitoring of metal components still face significant challenges in environmental adaptability [29, 30]. Integrating electrochemical monitoring with other physical methods to develop hybrid in-situ detection sensors for metal components holds promise for enhancing the accuracy of corrosion monitoring.

This study investigates the electrochemical corrosion behavior of protective coatings driven by electrochemical technology, using composite coatings (graphene/fluorocarbon coating) as an example. A laboratory cyclic accelerated test was designed, with one cycle comprising "UV/condensation + neutral salt spray + low-temperature exposure." Polarization curve analysis and AC impedance spectroscopy were employed to study the electrochemical corrosion behavior of the coatings. Combining polarization curves and electrochemical impedance spectroscopy, the corrosion behavior of graphene/fluorocarbon coatings with varying graphene contents in 3.5% NaCl solution was analyzed. Performance evaluations of the composite coating were conducted through hardness, adhesion, and impact resistance tests. Based on the analysis results, the optimal formulation for the graphene/fluorocarbon coating was determined.

2 | Corrosion monitoring and performance evaluation of protective coatings

2.1 | Types and characteristics of protective coatings

Coating technology is an effective means of protecting metal surfaces. Commonly used coatings include:

1) Oxide coatings: By controlling temperature, a stable oxide layer such as Al_2O_3 or Cr_2O_3 is formed on the metal surface. These oxide layers effectively isolate the metal from direct contact with corrosive media, thereby reducing the corrosion rate.

2) Thermal spray coatings: Utilizing high-velocity gas streams to spray molten materials onto metal surfaces, forming dense, uniform protective layers. Common thermal spray materials include nickel-based, cobalt-based metals, and ceramics.

3) Diffusion coatings: Through high-temperature treatment, externally added elements (such as aluminum, chromium, etc.) form rich protective layers on the metal surface, enhancing corrosion resistance.

4) Composite coatings: Combine the above techniques to create dual-layer or multi-layer protective layers, leveraging the advantages of various coatings to achieve optimal protection.

2.2 | Corrosion testing and coating performance evaluation

Comprehensive testing of coating performance is essential to ensure its stability and durability in practical applications. Once the coating is applied, microscopic examination becomes the primary step, not only facilitating observation of the coating's microstructure but also confirming whether its distribution and thickness are uniform. To ensure the coating functions properly in real-world environments, it is placed in a corrosive environment to fully simulate actual usage conditions. This simulated testing provides extensive information about the coating's performance. After a fixed exposure period, samples are retrieved and subjected to advanced electrochemical techniques to yield detailed data on corrosion progression.

To comprehensively evaluate coating performance, additional tests assess hardness, adhesion, and impact resistance. Hardness testing evaluates wear resistance. Adhesion testing ensures the coating bonds firmly to the substrate without detaching under external forces. Impact resistance testing verifies stability against sudden external shocks. This rigorous testing series guarantees superior coating performance across diverse environments and conditions.

3 | Experimental design

This study employs a widely used composite coating for experimental simulation. It simulates the electrochemical corrosion behavior of graphene/fluorocarbon coatings with varying graphene contents in seawater, investigating the corrosion resistance and degradation mechanisms of fluorocarbon (FEVE) coatings [31].

3.1 | Coating preparation

The substrate for the test specimens consists of Q235 steel with dimensions of 1 cm × 1 cm × 1 cm. After undergoing sandblasting (Sa2½) and degreasing treatment, the surface is coated with graphene/fluorocarbon coatings containing varying amounts of graphene. The total coating thickness is (35±8) μm, with the primer layer at (18±5) μm and the topcoat at (23±5) μm.

3.2 | Accelerated test method

Tests were conducted according to the methods specified in ISO 20340-2003 "Paints and varnishes—Performance requirements for protective coating systems for offshore structures and associated structures." The accelerated cycling test items are listed in Table 1. The equipment used for testing included a B-UV-II UV weathering tester, an LYW-025 salt spray corrosion tester, and a Hisense BCD-203FH refrigerator.

TABLE 1 Cyclic accelerated test

Time	Items of test	Condition
Day 1∼3	UV/condensation	4 h UV (60 ℃, 0.68 W/m^2)/4h condensation (50 ℃)
Day 4∼6	Neutral salt spray	5%NaCl solution Spray quantity: 1∼2 mL/ (h 80cm^2)
Day 7	Exposure to lowtemperature	(-20±2) ℃

3.3 | Test methods

3.3.1 | Polarization curve measurement

Polarization curves are primarily used to express the relationship between electrode corrosion current density and electrode corrosion potential. By measuring, analyzing, and calculating the polarization processes of anodes and cathodes, fundamental kinetic parameters of electrode reactions can be obtained. This enables the evaluation of an electrode metal's polarization capability in relevant corrosive media and reveals the patterns and mechanisms of galvanic corrosion. By measuring polarization curves, the anodic and cathodic Tafel slopes of electrode metals can be calculated. Subsequently, the galvanic potential and galvanic current of the couple can be determined based on the intersection point of the anodic reaction polarization curve of the anodic metal and the cathodic reaction polarization curve of the cathodic metal. This enables the assessment of the corrosion rate of the anodic metal [32].

3.3.2 | Electrochemical impedance measurement

Electrochemical impedance spectroscopy (EIS) is a crucial in-situ measurement technique for studying galvanic corrosion. It provides fundamental electrochemical information about the interface between the metal under test and the corrosive electrolyte. By fitting EIS data to equivalent circuits, corresponding kinetic parameters can also be obtained [33]. The fundamental principle of EIS testing is as follows: When the electrode system is in a stable steady state, it is perturbed during the test process using sinusoidal polarization signals $\Delta\varphi$ of varying frequencies but constant amplitude. The resulting ΔI response values for current density are measured. Ultimately, when $\Delta\varphi$ and ΔI satisfy three basic conditions—stability, causality, and linearity—the impedance and admittance spectra of the test system can be determined. These are categorized into impedance spectra and admittance spectra. Electrochemical impedance spectroscopy is commonly employed in general electrochemical research. Crucially, unlike polarization curve measurements that degrade the tested metal, EIS constitutes a non-destructive test conducted under equilibrium conditions. Its broad frequency range (typically 10^{-3} to 10^{5} Hz) simplifies computational analysis of electrode system dynamics and diffusion processes.

3.3.3 | Hardness testing

This study employed the QHQ-A portable pencil scratch tester, referencing the "Pencil Method for Determining the Hardness of Paint and Varnish Films" (GB/T 6739-2022), to measure the hardness of fluorocarbon coatings through their pencil hardness grades. A pencil lead of varying hardness grades was pressed downward at a 45° angle onto the coating surface under a load of 7.36±0.13 N. Holding the wheel axle between thumb and index finger, the tester was moved across the coating surface at a slow, uniform speed. The test result was visually assessed.

3.3.4 | Adhesion test

This study employs the PosiTest AT-A pull-off adhesion tester to evaluate the bond strength between coatings and metal substrates. The testing apparatus consists of a digital pull-off tester and a set of specialized pull-off heads. It automatically calculates pull-off results based on mandrel size and utilizes bearing balls within the sleeve to rapidly lock the mandrel tip, ensuring precise positioning. This generates balanced pull-off force,

yielding accurate test results. Typically, the coating is first applied to the substrate and cured for later use. An AB adhesive is applied to firmly bond the test piece to the coating. A cutter matching the test piece size is then used to cut the coating down to the bare metal substrate. The test piece is subsequently locked in the pull-off head, and vertical pull-off force is applied to obtain the adhesion test results.

3.3.5 | Erosion resistance test

This study employed two accelerated erosion wear test apparatus to evaluate the erosion resistance of coatings. Test samples were prepared by applying the coating to 1cm×1cm×1cm Q235 steel plates, followed by curing to ensure uniform and complete coating coverage. To ensure accuracy in measuring coating thickness changes, a preliminary water saturation test can be conducted before erosion testing. This reduces the influence of coating water resistance while more realistically simulating water-sand erosion conditions. The coating specimens were sealed with adhesive on the back, leaving only one coated side exposed. After the adhesive dries, fully immerse the coated specimens in deionized water and measure the thickness at regular intervals. After a defined cycle, observe the thickness change pattern. Use the thickness after water saturation as the initial thickness before erosion testing, then proceed with the erosion test. Based on the test results and observations, the coating's erosion resistance can be evaluated more intuitively and efficiently, and differences between various coating samples can be compared.

4 | Results and discussion

4.1 | Electrochemical performance analysis

4.1.1 | Polarization curve

The polarization curves for different coatings are shown in Figure 1. The corrosion potential and corrosion current density were obtained using the Tafel fitting method [34], as presented in Table 2, which indicates that electrodes coated with graphene/fluorocarbon exhibit a significantly positive shift in corrosion potential and reduced corrosion current density compared to FEVE-coated electrodes. This demonstrates that graphene incorporation effectively enhances the protective performance of the coating, primarily due to the layered structure of graphene effectively impeding the penetration and erosion of corrosive media within the coating. Furthermore, the corrosion current density of the FEVE coating is 6.133×10^{-6} A/cm^2, while the FEVE-0.5%G coating exhibited a corrosion current density of 2.366×10^{-10} A/cm^2, demonstrating the best protective performance. When the graphene content reached 0.9%, the protective efficacy of the coating decreased. This decline was primarily attributed to graphene agglomeration, where filler clustering led to defects such as cracks and voids in the coating, thereby impairing its protective properties.

4.1.2 | AC impedance spectrum

To investigate the coating failure process, alternating current impedance spectroscopy (EIS) was employed to test the coatings. To analyze the effect of graphene content on the corrosion resistance of the coatings, the EIS spectra were fitted using equivalent circuits. The equivalent circuit diagrams are shown in Figure 2, where (a) to (c) represent the equivalent circuits selected for the initial, intermediate, and late stages, respectively. In

the equivalent circuit, Rs denotes the solution resistance, Rc represents the coating resistance, Rct signifies the charge transfer resistance, Zw indicates the impedance diffusion tail, Q denotes the constant phase angle element, Qc represents the coating capacitance, Qdl signifies the double layer capacitance, and n denotes the constant phase angle exponent.

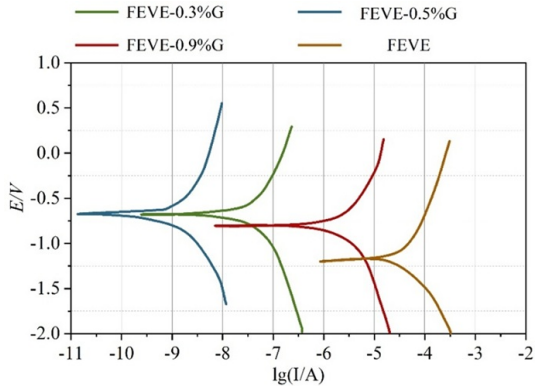

FIGURE 1 Polarization curve of different coatings

TABLE 2 Fitted results of polarization curves

Samples	Jcorr/ (A•cm^{-2})	E_{corr}/V
FEVE	6.133×10^{-6}	-0.9244
FEVE-0.3%G	6.252×10^{-9}	-0.5234
FEVE-0.5%G	2.366×10^{-10}	0.4412
FEVE-0.9%G	3.019×10^{-7}	0.5547

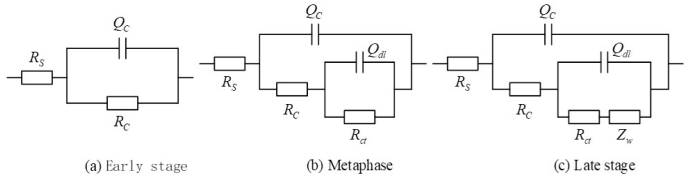

FIGURE 2 Equivalent circuit diagram

The electrochemical impedance spectra of the FEVE coating are shown in Figure 3. Figure 3(a) to (c) represent the EIS plots of the fluorocarbon coating during the initial, intermediate, and late stages of immersion in a 3.5% NaCl solution, respectively. During the initial immersion stage, the impedance spectrum exhibited two time constants. The FEVE coating can be fitted using the equivalent circuit diagram in Figure 2(c), with lg(|Z|0.01) values ranging from 104.5 to 103.5 $\Omega \cdot \mathrm{cm}^2$. This phase corresponds to the late immersion stage, representing the coating's corrosion failure phase. The corrosive medium rapidly penetrates the coating to

reach the stainless steel surface, initiating electrochemical reactions. Visible rusting becomes discernible on the coating surface at this point. Continued immersion accelerates the corrosion rate of the metal substrate, with corrosion products accumulating on the electrode surface to form a diffusion layer, resulting in the appearance of a diffusion arc.

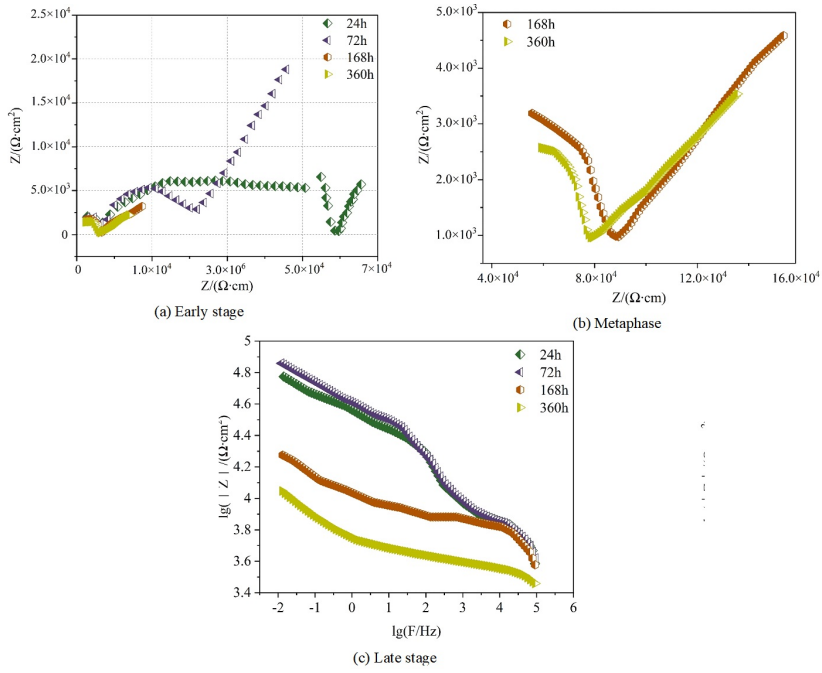

FIGURE 3 EIS of FEVE coating under different immersion times in 3.5%NaCl solution

The electrochemical impedance spectra of graphene/fluorocarbon coatings with different graphene contents after immersion in 3.5% NaCl solution for varying durations are shown in Figures 4, 5 and 6. Figures 4(a)–(c) present the electrochemical impedance spectra of the FEVE-0.3%G coating. Figures 5(a) to 5(c) present the electrochemical impedance spectra of the FEVE-0.5%G coating, while Figures 6(a) to 6(c) display those of the FEVE-0.9%G coating.

In Figure 4(a), the FEVE-0.3%G coating exhibits a single capacitive arc in the high-frequency region of the impedance spectrum after 24 hours of immersion, characterized by a single time constant. Continued immersion causes the coating impedance spectrum to transition to two time constants. Entering the mid-immersion phase, this stage can be fitted using the model in Figure 2(b). In Figure 4(c), lg(|Z|0.01) ranged from 106.8 to 105.4 $\Omega \cdot \mathrm{cm}^2$, indicating that the coating retained a certain level of protective efficacy even after 360 hours of immersion.

As shown in Figures 5(a) and 5(b), after 24 hours of immersion, the Nyquist plot of the FEVE-0.5%G coating exhibits a straight line with an inclination angle close to 90°, and the lg(|Z|0.01) value exceeds 10^{10} $\Omega \cdot \mathrm{cm}^2$. At this stage, the coating provides excellent protection for the substrate, effectively shielding against the penetration of corrosive media. As immersion time increases, the FEVE-0.5%G coating exhibits single capacitive impedance. The longer the immersion duration, the smaller the capacitive arc radius becomes.

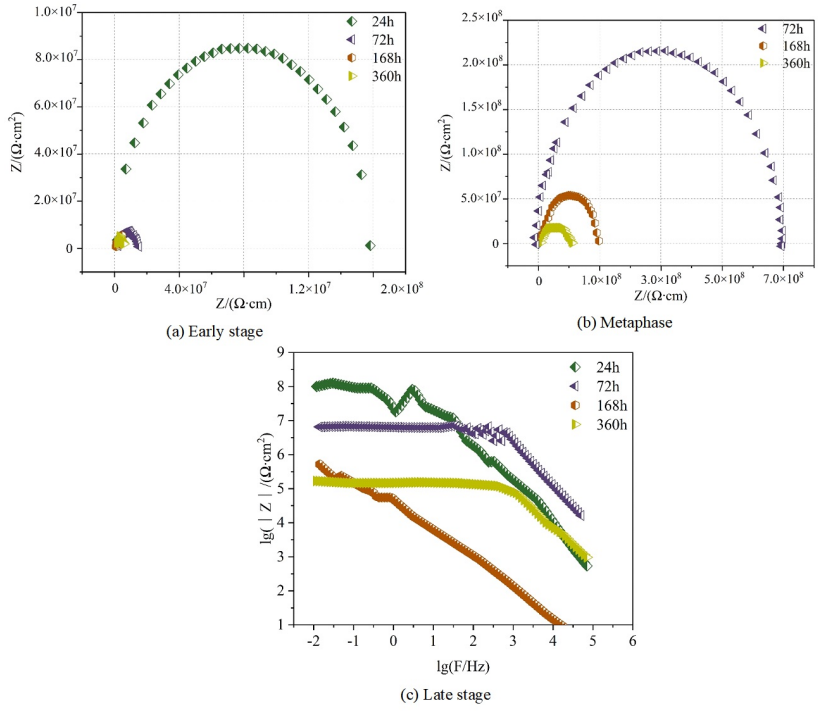

FIGURE 4 EIS of FEVE-0.3%G coating under different immersion times

Throughout the entire immersion process, only one time constant appears on the EIS spectrum, which can be fitted using the model in Figure 2(a). This stage represents the initial immersion phase. As shown in Figure 5(c), throughout the immersion process, the value of lg(|Z|0.01) changes from 1010 $\Omega \cdot cm^2$ to 107.6 $\Omega \cdot cm^2$. At this point, the coating exhibits good protective performance.

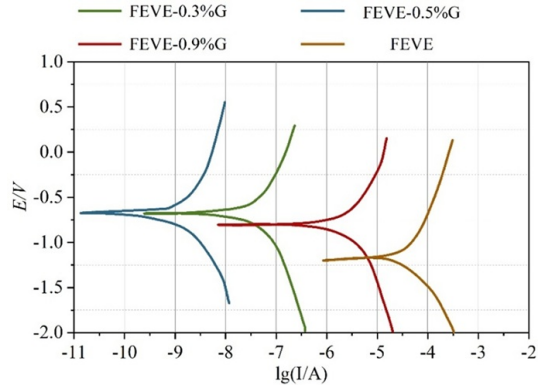

FIGURE 5 EIS of FEVE-0.5%G coating under different immersion times

As shown in Figures 6(a) to 6(c), during the 0 to 360-hour immersion process, the impedance spectrum of the FEVE-0.9%G coating exhibits a large capacitive arc in the high-frequency region and a trailing arc in the low-frequency region. Furthermore, the radius of the capacitive arc gradually decreases with increasing immersion time. During this immersion process, the value of lg(|Z|0.01) changes from 107.3 $\Omega \cdot cm^2$ to 105.8 $\Omega \cdot cm^2$. This indicates that electrolyte has permeated the coating/metal interface during immersion, though no macroscopic pores have yet formed on the coating surface. This stage represents the coating's water penetration phase, which can be fitted using the model in Figure 2(b). It corresponds to the mid-immersion period, during which the coating still maintains excellent protective performance.

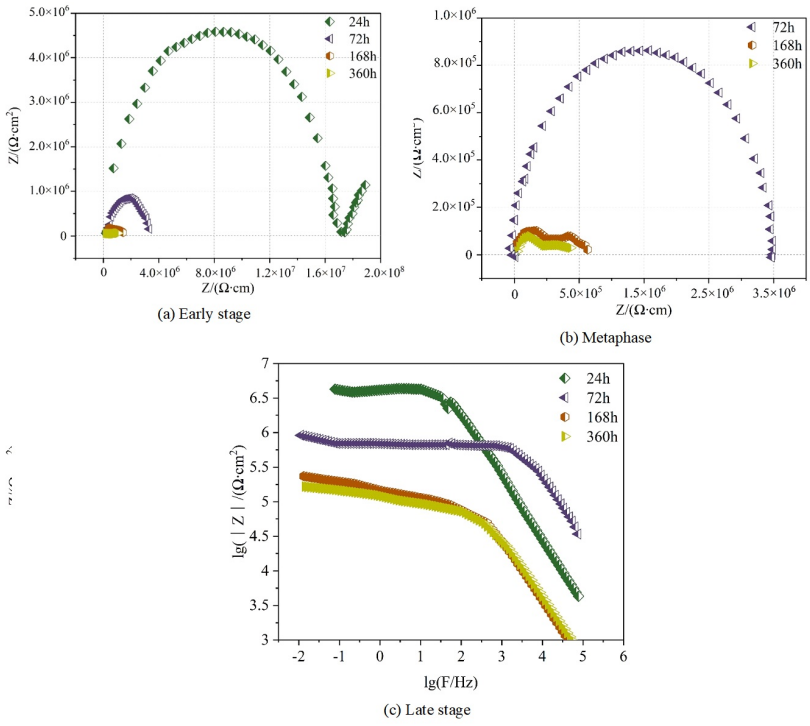

FIGURE 6 EIS of FEVE-0.9%G coating under different immersion times

The optimal graphene content is consistently 0.5%. When the content is too low, it fails to effectively impede the penetration of corrosive media. Conversely, when the content is too high, it creates partial corrosion pathways, thereby reducing the coating's anti-corrosion performance.

4.2 | Performance evaluation

4.2.1 | Hardness comparison analysis

The hardness comparison of different coatings is shown in Table 3. Comparing the hardness results of FEVE, FEVE-0.3%G, FEVE-0.5%G, FEVE-0.9%G, epoxy coal tar paint (C1), and single-component fluorocarbon waterproof coating (C2), it is evident that the FEVE-0.5%G coating exhibits the highest hardness, while the

FEVE coating is the softest. This indicates that higher graphene content leads to significant brittleness and cracking in the coating, while lower content results in insufficient curing and excessive softness. Therefore, the fluorocarbon coating selected in this section is the FEVE-0.5%G coating, which exhibits good hardness and a smooth, flat appearance. Comparing the hardness of the FEVE-0.5%G coating against industrial-grade epoxy coal tar paint and single-component fluorocarbon waterproof coatings reveals that FEVE-0.5%G also outperforms both industrial products in hardness, demonstrating potential wear resistance. To further evaluate the coating's fundamental properties, adhesion and erosion resistance tests were conducted comparing the FEVE-0.5%G coating with the other two industrial products.

TABLE 3 Hardness contrast of different coating

Coating name	Hardness
FEVE	1B
FEVE-0.3%G	2B
FEVE-0.5%G	3B
FEVE-0.9%G	2B
C1	2B
C2	2B

4.2.2 | Adhesion comparison analysis

Adhesion tests were conducted on the confirmed FEVE-0.5%G coating and two other industrial products. Each coating sample underwent five tests, with the average value recorded. The adhesion results are shown in Table 4. It was found that the adhesion strength between the FEVE-0.5%G coating and the Q235 carbon steel substrate reached 4.49 MPa, exceeding twice the adhesion strength of the other two industrial products. This indicates the FEVE-0.5%G coating possesses superior crosslinking density, confirming its strong bonding capability with carbon steel substrates. The coating adheres more firmly to the substrate surface, effectively shielding it from external environmental corrosion and damage. Additionally, this reduces the risk of coating detachment and flaking, contributing to the coating's integrity and stability. By reducing abrasive wear from water-sand erosion and mitigating damage from corrosive media to steel structures, the FEVE-0.5%G coating extends the service life of steel structures while lowering maintenance costs and safety risks.

TABLE 4 Contrast of adhesion of different coating

Coating name	Adhesion/Mpa
FEVE-0.5%G	4.49
C1	2.02
C2	2.24

4.2.3 | Erosion resistance analysis

The determined FEVE-0.5%G coating and two other industrial coatings underwent erosion resistance testing. The accelerated erosion wear test apparatus was activated, and changes in adhesion and thickness for each coating sample were recorded post-experiment. The coatings' erosion resistance capabilities were discussed, with results averaged from three or more measurements per sample. Changes in adhesion and thickness before and after 54 hours of erosion are shown in Table 5. It can be observed that the adhesion of the single-component fluorocarbon waterproof coating exhibits significant variation. During water-sand erosion, the adhesion between the coating and the Q235 carbon steel substrate decreases, potentially allowing corrosive media to reach the steel surface more readily and causing interfacial damage to the steel. The epoxy coal tar paint also exhibited substantial adhesion variation. Its bonding strength with the Q235 carbon steel substrate diminished during water-sand erosion, particularly with significant thickness reduction post-erosion. This correlates with the coating's soft hardness and low adhesion properties, indicating that under water-sand impact, the epoxy coal tar paint is prone to erosion wear causing coating delamination, demonstrating poor erosion resistance. The FEVE-0.5%G coating exhibited the smallest changes in both adhesion and thickness after erosion. This indicates that under certain water-sand erosion conditions, the coating maintains relatively stable surface structure and adhesion properties, resulting in superior wear resistance and abrasion resistance. Compared to the other two industrial coatings, it demonstrates better protective efficacy against erosion.

TABLE 5 Change of adhesion and thickness before and after erosion

Coating name	Pre-erosion adhesion/Mpa	Post-erosion adhesion/Mpa	Thickness variation/μm
FEVE-0.5%G	4.49	4.26	10.2
C1	2.02	1.45	83.5
C2	2.24	1.02	45.6

5 | Conclusion

The study employed AC impedance spectroscopy and dynamic polarization curves to investigate the electrochemical corrosion behavior and failure mechanisms of composite coatings in simulated seawater, yielding the following conclusions:

(1) Graphene significantly enhances the corrosion resistance of fluorocarbon coatings. A graphene content of 0.5% in graphene/fluorocarbon coatings effectively blocks corrosion liquid penetration, providing optimal protection for Q235 steel substrates. When the content is too low, it fails to effectively block corrosion medium penetration; when too high, it creates partial corrosion pathways, reducing the coating's anti-corrosion performance.

(2) Performance tests revealed that the FEVE-0.5%G coating exhibited the best relative properties. The FEVE-0.5%G coating was tested against two other industrial coatings for hardness, adhesion, and erosion resistance. Analysis of hardness, adhesion, and erosion resistance test results revealed that the FEVE-0.5%G coating exhibits moderate hardness, good adhesion to the Q235 substrate, and superior fundamental properties compared to the other two coatings. It maintained stable adhesion under water-sand erosion conditions with minimal thickness change post-erosion. This indicates that the FEVE-0.5%G coating possesses good wear

resistance and erosion resistance, making it suitable as a base coating for composite coatings.

References

[1] Hou, B., Li, X., Ma, X., Du, C., Zhang, D., Zheng, M., ... & Ma, F. (2017). The cost of corrosion in China. *NPJ Materials Degradation, 1*(1), 4.

[2] El-Enin, S. A., & Amin, A. (2015). Review of corrosion inhibitors for industrial applications. *International Journal of Energy Research, 3*(2), 127-145.

[3] Aljibori, H. S., Alamiery, A., & Kadhum, A. A. H. (2023). Advances in corrosion protection coatings: A comprehensive review. *International Journal of Corrosion and Scale Inhibition, 12*(4), 1476-1520.

[4] Fotovvati, B., Namdari, N., & Dehghanghadikolaei, A. (2019). On coating techniques for surface protection: A review. *Journal of Manufacturing and Materials processing, 3*(1), 28.

[5] Thomas, D., R, R., Philip, E., Sindhu, R., Ulaeto, S. B., Pugazhendhi, A., & Awasthi, M. K. (2022). Developments in smart organic coatings for anticorrosion applications: a review. *Biomass Conversion and Biorefinery, 12*(10), 4683-4699.

[6] Hu, R. G., Zhang, S., Bu, J. F., Lin, C. J., & Song, G. L. (2012). Recent progress in corrosion protection of magnesium alloys by organic coatings. *Progress in Organic Coatings, 73*(2-3), 129-141.

[7] Lyon, S. B., Bingham, R., & Mills, D. J. (2017). Advances in corrosion protection by organic coatings: What we know and what we would like to know. *Progress in Organic Coatings, 102*, 2-7.

[8] Chhipa, S. M., Sharma, S., & Bagha, A. K. (2024). Recent development in polymer coating to prevent corrosion in metals: A review. *Materials Today: Proceedings*.

[9] Zajec, B., Bajt Leban, M., Kosec, T., Kuhar, V., Legat, A., Lenart, S., ... & Gavin, K. (2018). Corrosion monitoring of steel structure coating degradation. *Tehnički vjesnik, 25*(5), 1348-1355.

[10] Farh, H. M. H., Seghier, M. E. A. B., & Zayed, T. (2023). A comprehensive review of corrosion protection and control techniques for metallic pipelines. *Engineering Failure Analysis, 143*, 106885.

[11] Liu, G., & Wheat, H. G. (2009). Use of a fluorescent indicator in monitoring underlying corrosion on coated aluminum 2024-T4. *Journal of the Electrochemical Society, 156*(4), C160.

[12] El-Nahhal, I. M., Zourab, S. M., & El-Ashgar, N. M. (2001). Encapsulation of phenolphthalein pH-indicator into a sol-gel matrix. *Journal of Dispersion Science and Technology, 22*(6), 583-590.

[13] Rahman, Z., & Das, S. K. (2021). Ionic Liquids based Acid-base Indicators for Aqueous to the Non-Aqueous Medium: An Overview. *Chemistry Select, 6*(34), 9164-9174.

[14] Antina, E. V., Bumagina, N. A., V'yugin, A. I., & Solomonov, A. V. (2017). Fluorescent indicators of metal ions based on dipyrromethene platform. *Dyes and Pigments, 136*, 368-381.

[15] Maia, F., Tedim, J., Bastos, A. C., Ferreira, M. G. S., & Zheludkevich, M. L. (2013). Nanocontainer-based corrosion sensing coating. *Nanotechnology, 24*(41), 415502.

[16] Liu, X., Spikes, H., & Wong, J. S. (2014). In situ pH responsive fluorescent probing of localized iron corrosion. *Corrosion Science, 87,* 118-126.

[17] Chen, C., Yu, M., Tong, J., Xiong, L., Li, Y., Kong, X., ... & Li, S. (2022). A review of fluorescence based corrosion detection of metals. *Corrosion Communications, 6*, 1-15.

[18] Pidaparti, R. M., Neblett, E. B., Miller, S. A., & Alvarez, J. C. (2007). Monitoring the corrosion process of Al alloys through pH induced fluorescence. *Smart Materials and Structures, 17*(1), 015001.

[19] Liu, T., Zhang, D., Ma, L., Huang, Y., Hao, X., Terryn, H., ... & Li, X. (2022). Smart protective coatings with self-sensing and active corrosion protection dual functionality from pH-sensitive calcium carbonate microcontainers. *Corrosion Science, 200*, 110254.

[20] Tian, X. L., Feng, C., & Zhao, X. H. (2020). Corrosion monitoring effect of rhodamine-ethylenediamine on copper relics under a protective coating. *ACS Omega, 5*(34), 21679-21683.

[21] Sun, K., Zhong, W., Huang, S., He, X., Cai, W., Ma, R., ... & Li, W. (2025). Research Progress on the Corrosion Mechanism and Protection Monitoring of Metal in Power Equipment. *Coatings, 15*(2), 119.

[22] Wang, X., Jin, L., Wang, J., Wang, R., Liu, X., Gao, K., ... & Zhang, D. (2025). Assessing the corrosion protection property of coatings loaded with corrosion inhibitors using the real-time atmospheric corrosion monitoring technique. *International Journal of Minerals, Metallurgy and Materials, 32*(1), 119-126.

[23] Latif, J., Khan, Z. A., & Stokes, K. (2020). Structural monitoring system for proactive detection of corrosion and coating failure. *Sensors and Actuators A: Physical, 301*, 111693.

[24] Davis, G. D., Vargo, T. G., Dalgleish, A. W., & Deason, D. (2004). Corrosion protection and condition monitoring using 'Smart'appliques. *Materials performance, 43*(8), 32-36.

[25] Zamarreño, C. R., Rivero, P. J., Hernaez, M., Goicoechea, J., Matías, I. R., & Arregui, F. J. (2015). Optical sensors for corrosion monitoring. *Intelligent Coatings for Corrosion Control*, 603-640.

[26] Cook, D. C. (2005). Spectroscopic identification of protective and non-protective corrosion coatings on steel structures in marine environments. *Corrosion Science, 47*(10), 2550-2570.

[27] Augustyniak, A., Tsavalas, J., & Ming, W. (2009). Early detection of steel corrosion via "turn-on" fluorescence in smart epoxy coatings. *ACS Applied Materials & Interfaces, 1*(11), 2618-2623.

[28] Xia, T. F., Zhang, L., Zhang, D. Q., & Gao, L. X. (2015). Detection of T91 Steel Corrosion with a Fe3+-Enhanced Fluorescence Probe. *Journal of Chemistry, 2015*(1), 654802.

[29] Komary, M., Komarizadehasl, S., Tošić, N., Segura, I., Lozano-Galant, J. A., & Turmo, J. (2023). Low-cost technologies used in corrosion monitoring. *Sensors, 23*(3), 1309.

[30] Li, L., Chakik, M., & Prakash, R. (2021). A review of corrosion in aircraft structures and graphene-based sensors for advanced corrosion monitoring. *Sensors, 21*(9), 2908.

[31] Li, L., Guo, X. C., & Zhou, Y. Y. (2011). The research of chemical resistance for air curing FEVE fluorocarbon coatings. *Advanced Materials Research, 239*, 944-948.

[32] Galvez-Vazquez, M. D. J., Grozovski, V., Kovács, N., Broekmann, P., & Vesztergom, S. (2020). Full model for the two-step polarization curves of hydrogen evolution, measured on RDEs in dilute acid solutions. *The Journal of Physical Chemistry C, 124*(7), 3988-4000.

[33] Zala, P., Tripathi, B., Khemnani, M., Hirpara, D., Kapadia, R., Gupta, M., ... & Kumar, M. (2025). Optimizing anti-reflection coating using electrochemical impedance spectroscopy to enhance electrical performance of solar cell. *Optical and Quantum Electronics, 57*(8), 1-19.

[34] Coduto, J. R., & Leddy, J. (2021, May). (General Student Poster Session Winner-1st Place) An Algorithm for Fitting Tafel Data and Determining Kinetic Parameters. In *Electrochemical Society Meeting Abstracts 239* (No. 51, pp. 2019-2019). The Electrochemical Society, Inc..